International Journal of Automotive Technology, Vol. 8, No. 4, pp. 521–531 (2007)

1229–9138/2007/035–15

ANALYSIS OF DOPPLERIZED ACCELERATION SIGNALS IN A ROTATING SHAFT BY USING A VOLD-KALMAN ORDER TRACKING FILTER

H. S. KOOK[1)*] and C. CRANE[2)]

[1)]School of Mechanical and Automotive Engineering, Kookmin University, Seoul 136-702, Korea
[2)]Department of Mechanical and Aerospace Engineering, University of Florida, Gainesville, FL32611, U.S.A.

(Received 19 April 2007; Revised 16 June 2007)

ABSTRACT–Measurement of the vibration transmitted through rotating shafts such as halfshafts in vehicles is of interest in applications such as noise transfer analysis and the study of operating deflections. Vibration signals transmitted through a rotating shaft usually include six degree-of-freedom components, thus making the measurement of vibration a challenging task. In the present work, a new measurement method is presented, one that resolves the minimum of only two one-axis accelerometer signals into all components of vibration with reasonable accuracy. The method utilizes the Dopplerized signals obtained from accelerometers attached to a rotating shaft and a Vold-Kalman order tracking filter to decompose signals into orders of different vibration components. The new method proposed in the present work is verified by simulated run-up test data and applied to an experimentally obtained data set.

KEY WORDS : Rotating shaft vibration, Doppler effects, Vold-Kalman order tracking filter

1. INTRODUCTION

In the early stage of noise, vibration, and harshness (NVH) development or the later stage of NVH refinement or troubleshooting for a vehicle, it is often necessary to measure the vibrations of a drivetrain system to understand the noise and vibration contribution transmitted from the engine to the interior of the vehicle (Suh and Orzechowski, 2003; Williams and Wilson, 1997). The noise and vibration sources are usually identified by order tracking analysis of a run-up or run-down test. The order tracking analysis (Gade *et al.*, 1995) is a useful tool when sinusoidal frequencies of major contributors are multiples of that of a fundamental tone (i.e., the engine rpm in the NVH applications).

Measurement of vibration components in a rotating shaft could be a challenging task because six vibration components are involved (Figure 1) and all should be measured for rotating shafts. There are two methods for a vibration measurement of rotating shafts. One method uses contacting sensors such as accelerometers and strain gages, along with slip rings which allow the transmission of electrical signals from a rotating structure to a stationary structure. The other measurement method uses non-contact optical sensors such as laser Doppler vibrometry (LDV) and is generally considered more advanced since the method does not require modification of the rotating shafts due to installation of contacting sensors. This second method has been more popularly studied (Halliwell *et al.*, 1984; Wang *et al.*, 1992; Halliwell *et al.*, 1997; Miles *et al.*, 1999; Rothberg and Bell, 2004).

LDV measurement methods, however, sometimes have disadvantages over traditional measurement methods with contacting sensors. For instance, LDV measurements of a target vibration component require aligning the laser beam at specific angles. Therefore, measurements of all of the six degree-of-freedom vibration components could be a time-consuming task with a limited number of LDVs. Moreover, limited access to the rotating shaft sometimes does not allow for the necessary alignment at all.

The vibration measurement methods for rotating shafts using contacting sensors have been used to measure only part of the vibration component, for instance the rotational vibration component by using a pair of accelerometers attached axisymetrically in the circumferential directions. No attempts have been made to measure all six degree-of-freedom vibration components. In the present work, a new measurement method is proposed that uses two one-axis accelerometers to obtain orders of six degree-of-freedom vibration components simultaneously. It is proven theoretically and verified by experimental data that an accelerometer attached in either the axial or circumfer-

**Corresponding author.* e-mail: kook@kookmin.ac.kr

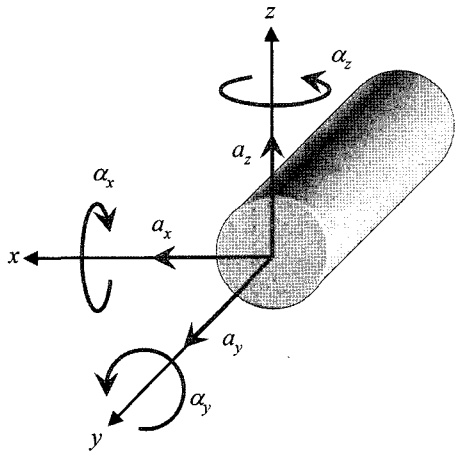

Figure 1. Three translational and three rotational vibration components transmitted across a cross-section of a rigid shaft.

ential directions of a rotating shaft measures three different vibration components, and, due to Doppler effects, orders of each of the vibration components can be retrieved with reasonable accuracy by utilizing the spread of the orders in a spectrogram.

2. KINEMATIC ANALYSIS

2.1. Definition of Body Coordinate System and Representation of Angular Motion

A body coordinate system is introduced to formally describe the three degree-of-freedom rotational motion of a disk. The body coordinate system used in the present work is shown in Figure 2. An intermediate coordinate system *x-y-z* is obtained by first rotating the global coordinate system *X-Y-Z* by angle ϕ about the *Z*-axis, and then rotating the resultant coordinate system by angle θ about the *x*-axis. Finally, the body coordinate system *1-2-3* is obtained by rotating the *x-y-z* coordinate system about the *y*-axis by angle ψ.

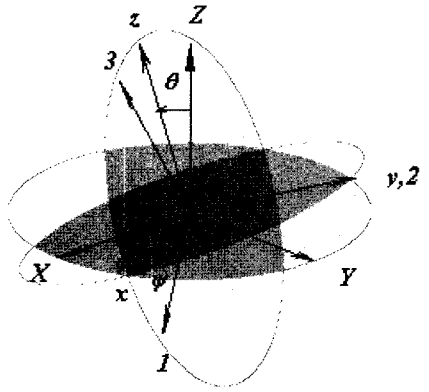

Figure 2. Global and local body coordinate systems.

Consider a rotating shaft whose circular cross-section lies on the *1-3* plane with its center at the origin, and which rotates about the *1-3* normal axis. The angular velocity of the disk (circular cross-section of the shaft) can then be represented by the combination of the first time-derivatives of the three angles: i.e.,

$$\boldsymbol{\omega}=\dot{\phi}\boldsymbol{u}_Z+\dot{\theta}\boldsymbol{u}_x+\dot{\psi}\boldsymbol{u}_2\,, \tag{1}$$

where $\boldsymbol{u}_Z$, $\boldsymbol{u}_x$, $\boldsymbol{u}_2$ denote unit vectors in the *Z*-, *x*-, and *2*-axes, respectively. In Figure 2, it can be seen that unit vectors are related to others as follows:

$$\boldsymbol{u}_Z=\boldsymbol{u}_z\cos\theta+\boldsymbol{u}_2\sin\theta, \tag{2}$$

$$\boldsymbol{u}_x=\boldsymbol{u}_X\cos\phi+\boldsymbol{u}_Y\sin\phi, \tag{3}$$

$$\boldsymbol{u}_x=\boldsymbol{u}_1\cos\psi+\boldsymbol{u}_3\sin\psi, \tag{4}$$

$$\boldsymbol{u}_z=\boldsymbol{u}_3\cos\psi-\boldsymbol{u}_1\sin\psi. \tag{5}$$

The angular velocity of the disk can be represented in terms of the basis vectors for the global coordinate system by using the relationship expressed in Equations (2) to (5), and can be written as:

$$\boldsymbol{\omega}=(\dot{\theta}\cos\phi-\dot{\psi}\cos\theta\sin\phi)\boldsymbol{u}_X +(\dot{\theta}\sin\phi-\dot{\psi}\cos\theta\cos\phi)\boldsymbol{u}_Y+(\dot{\phi}+\dot{\psi}\sin\theta)\boldsymbol{u}_Z\,. \tag{6}$$

By differentiating Equation (6) with respect to time, the angular acceleration of the disk can be easily obtained. Small amplitude vibration of a rotating shaft, a simpler form, which carries the assumption that angles ϕ and θ are negligibly small, is of interest and can be approximated as:

$$\boldsymbol{\alpha}\approx(\ddot{\theta}-\dot{\psi}\dot{\phi})\boldsymbol{u}_X+(\ddot{\psi}+\dot{\theta}\dot{\phi})\boldsymbol{u}_Y+(\ddot{\phi}+\dot{\psi}\dot{\theta})\boldsymbol{u}_Z\,. \tag{7}$$

By using transform relations represented by Equations (2) to (5), the angular velocity and acceleration expressed in the global coordinate system in Equations (6) and (7), respectively, can easily be transformed to the body coordinate system.

2.2. Acceleration of a Point on a Rotating Shaft

The acceleration of a point attached to a rigid body can be represented by the formula:

$$\boldsymbol{a}=\boldsymbol{a}_o+\boldsymbol{\alpha}\times\boldsymbol{r}+\boldsymbol{\omega}\times(\boldsymbol{\omega}\times\boldsymbol{r})\,, \tag{8}$$

where $\boldsymbol{r}$ is the position vector of the point from the origin of the global coordinate system, and $\boldsymbol{a}_o$ is the translational acceleration vector of the global coordinate system that can be expressed as:

$$\boldsymbol{a}_o=a_X\boldsymbol{u}_X+a_Y\boldsymbol{u}_Y+a_Z\boldsymbol{u}_Z \approx(a_X\cos\psi-a_Z\sin\psi)\boldsymbol{u}_1+a_Y\boldsymbol{u}_2+(a_X\sin\psi+a_Z\cos\psi)\boldsymbol{u}_3\,. \tag{9}$$

Consider a one-axis accelerometer attached at the coordinates of $(r_1,r_2,0)$ with its axis directed toward the 2-axis

in the body coordinate system. The acceleration vector of the point in the body coordinate system can be obtained by first transforming all the relevant vectors into the body coordinate system and then evaluating Equation (8). Since the one-axis accelerometer is assumed to be attached in a direction parallel with the axis of the rotating shaft, the only acceleration component of interest is in the 2-axis and can be written as:

$$a_2=a_Y+r_1\ddot{\theta}\sin\psi+r_1\ddot{\phi}\cos\psi +2r_1\dot{\psi}(\dot{\theta}\cos\psi-\dot{\phi}\sin\psi)-r_2(\dot{\phi}^2+\dot{\theta}^2). \quad (10)$$

It can be seen in Equation (10) that an accelerometer attached in the axial direction measures the signal that is the sum of translational acceleration in the *Y*-direction and Dopplerized signals of the two angular accelerations about the *Z*- and *Y*-axes, as well as products of various angular velocities.

If a one-axis accelerometer is assumed to be mounted at the coordinates of $(r_1,0,0)$ and directed toward the *3*-axis in the body coordinate system, the signal it measures can be obtained similarly: i.e.,

$$a_3=a_X\sin\phi+a_Z\cos\phi-r_1(\ddot{\psi}+\dot{\theta}\dot{\phi}) +r_1(\dot{\phi}\cos\psi+\dot{\theta}\sin\psi)(\dot{\theta}\cos\psi-\dot{\phi}\sin\psi). \quad (11)$$

It can be seen in Equation (11) that a one-axis accelerometer attached toward the circumferential direction of a rotating shaft measures Dopplerized signals of the translational accelerations in the *X*- and *Z*-directions as well as the signal from the angular acceleration about the 3-axis (i.e., the axis of the rotating shaft).

The magnitudes of the fourth and fifth terms in Equation (10) and the fourth term in Equation (11) are negligibly small compared to the rest of the terms, provided that the angular displacement of the disk is very small. This can be deduced from the fact that the ratio of the square of the first time-derivatives of an angle to the second time-derivatives of an angle is $O(\varepsilon)$, where ε is the amplitude of the angular displacement in radians.

2.3. Order components of Dopplerized Signals

The first two terms in Equation (11) can be rewritten as:

$$a_X\sin\psi+a_Z\cos\psi=\mathrm{Re}\{(-ja_X+a_Z)\exp(j\psi)\}, \quad (12)$$

where Re{} returns real part of a complex number and $j=\sqrt{-1}$. Orders k_2 of the acceleration signals a_X and a_Z can be expressed as:

$$a_{X,k_2}=2\mathrm{Re}\{\boldsymbol{A}_{X,k_2}\boldsymbol{\Theta}_{k_2}\}=\boldsymbol{A}_{X,k_2}\boldsymbol{\Theta}_{k_2}+\boldsymbol{A}^*_{X,k_2}\boldsymbol{\Theta}_{-k_2}, \quad (13)$$

$$a_{Z,k_2}=2\mathrm{Re}\{\boldsymbol{A}_{Z,k_2}\boldsymbol{\Theta}_{k_2}\}=\boldsymbol{A}_{Z,k_2}\boldsymbol{\Theta}_{k_2}+\boldsymbol{A}^*_{Z,k_2}\boldsymbol{\Theta}_{-k_2}, \quad (14)$$

where $A_k(t)$ is the complex envelope of order component k, $\boldsymbol{\Theta}_k(t)$ is the phasor of order k, and $(\,)^*$ denotes the complex conjugate. Given an underlying axle speed $f(t)$ in terms of frequency in Hertz as a function of time t, the phasor of order k can be represented as:

$$\boldsymbol{\Theta}_k(t)=\exp\left(j2\pi k\int_0^t f(u)du\right), \quad (15)$$

where the time integral of the frequency yields the total angle traveled in radians. With an assumption that the rotating speed of the shaft is order k_1 of the underlying axle speed, Dopplerized signals for the order k_2 of the acceleration signals a_X and a_Z can be obtained by substituting Equations (13) and (14) into right hand side of Equation (12):

$$\mathrm{Re}\{(-j\boldsymbol{A}_{X,k_2}+\boldsymbol{A}_{Z,k_2})\boldsymbol{\Theta}_{k_2+k_1}\}+\mathrm{Re}\{(j\boldsymbol{A}_{X,k_2}+\boldsymbol{A}_{Z,k_2})\boldsymbol{\Theta}_{k_2-k_1}\}. \quad (16)$$

Note that the complex envelopes for the order k_2 of the translational acceleration signals are modulated by phasors of orders k_2+k_1 and k_2-k_1. Since the angular acceleration signal in Equation (11) will not be order-shifted, order k_2 components of signals associated with the translational acceleration and the signal associated with the angular acceleration will not lie on the same line, and thus will be distinguishable, for instance, in the spectrogram of the signal containing all the order components. The same is true for the case of the signal expressed in Equation (10), where orders k_2 of the signals associated with the two angular accelerations are order-shifted to orders k_2+k_1 and k_2-k_1, while order k_2 of the signal associated with the translational acceleration in the *Y*-direction is not order-shifted and remains as order k_2.

As can been seen in Equation (16), each order-shifted term contains two vibration components: the two rotational accelerations for the case of the accelerometer attached in the axial direction and the two translational accelerations for the case of the accelerometer attached in the circumferential direction. The two acceleration components can be retrieved from the pair of order-shifted complex envelopes: i.e.,

$$\boldsymbol{A}_{X,k_2}=\boldsymbol{D}_{k_2+k_1}+\boldsymbol{D}_{k_2-k_1}, \quad (17)$$

$$\boldsymbol{A}_{Z,k_2}=j(\boldsymbol{D}_{k_2+k_1}-\boldsymbol{D}_{k_2-k_1}), \quad (18)$$

where $\boldsymbol{D}_{k_2+k_1}$ is the complex envelope for order k_2+k_1, and can be represented as $\boldsymbol{D}_{k_2+k_1}=(-j\boldsymbol{A}_{X,k_2}+\boldsymbol{A}_{Z,k_2})/2$ and $\boldsymbol{D}_{k_2-k_1}$ is the complex envelope for order k_2-k_1 and can be represented as $\boldsymbol{D}_{k_2-k_1}=(j\boldsymbol{A}_{X,k_2}+\boldsymbol{A}_{Z,k_2})/2$.

It can be shown that the rest of the terms in Equations (10) and (11) can be decomposed into a constant signal and a signal of order $2k_2$. Since those terms contribute not at all to orders k_2-k_1, k_2, and k_2+k_1, and are negligible in magnitude compared to the first three terms as noted in section 2.2, the three translational and the three rotational accelerations can in theory be obtained with accuracy by using the method described in the present work.

3. SIMULATION

Since no attempt to directly measure the 6 components of vibration signals simultaneously at a cross section of a rotating shaft has been made to the authors' best knowledge, an experimental comparison and validation of the proposed method with a traditional experimental method is not possible. In this work, therefore, simulated signals that would have been obtained by the two accelerometers, one attached in the axial direction and the other attached in a circumferential direction of a cross-sectional disk of a rotating shaft, on a certain empirical condition, are used to see if the proposed method successfully retrieves the set of the given six components of vibration signals.

3.1. Simulated Signals

3.1.1. Simulated vibration signals

For simplicity of simulation, each of the 6 components of vibration is assumed to result from single degree-of-freedom systems. The impulse response of a single degree-of-freedom system can be represented as:

$$h(t)=Ae^{-\zeta\omega_n t}\sin\omega_d t, \tag{19}$$

where A is the amplitude of the impulse response, ζ is the damping ratio, and ω_n and ω_d are the natural and damped natural frequencies, respectively. The parameter sets used for each vibration component in the simulation are summarized in Table 1.

The output translational and/or rotational displacements, $y(t)$, can then be calculated by convolving the corresponding impulse response and the input force $x(t)$:

$$y(t)=x(t)\times h(t). \tag{20}$$

In the simulated run-up test, the input force is a linear combination of sweeping sine functions; a simple case of constant amplitude B and the sweep ratio γ is considered for simplicity of analysis:

$$x(t)=B\sin(\gamma t^2). \tag{21}$$

The simulated run-up test was performed with the engine speed varying from 700 to 2200 rpm with a constant sweep ratio, SR_{RPM}, of 50 rpm/s, and the system is assumed to be excited by only the second- and the fourth-order components. The amplitude of the second-order force was assumed to be a unit while the amplitude of the fourth-order force was assumed to be 5 dB less than that of the second-order force component. The input force can, therefore, be represented as:

$$x(t)=B_1\sin(\gamma_1 t^2)+B_2\sin(\gamma_2 t^2), \tag{22}$$

where B_1 and B_2 are a unit and 0.3162, respectively, and γ_1 and γ_2 are $2\times(2\pi)\times50/60$ and $4\times(2\pi)\times50/60$, respectively. The output acceleration can then be obtained by following the differentiation rule of convolution:

$$y''=x''\times h. \tag{23}$$

Table 1. Single degree-of-freedom impulse response parameters for each vibration component.

	translational components			rotational components		
	x	y	z	x	y	z
A (μm or °)	1	1	1	0.0015	0.0012	0.0015
f_n (Hz)	65	65	65	60	60	60
ζ	0.04	0.04	0.04	0.04	0.04	0.04

3.1.2. Dopplerized signals

To measure the six components of vibrations at a cross-section of a rotating shaft, one accelerometer is attached facing the axial direction while the other accelerometer is attached facing the circumferential direction, as described in section 2 (Figure 3). Since the vibration signals are measured while the two accelerometers are rotating with the shaft, some of the vibration signals are Dopplerized. In the simulated run-up test, the halfshaft is assumed to rotate at a proportional angular speed with the engine shaft by a ratio of 0.1444:1. The accelerometer mounted in the axial direction measures both the translational component of vibration in the y-direction and the Dopplerized rotational components of vibration about the x- and z-axes, while the accelerometer mounted in the circumferential direction measures the rotational component of vibration about the y-axis and the Dopplerized translational components of vibration in the x- and z-directions. The x-axis is in fact defined as the direction of the accelerometer as it is initially positioned, attached in the circumferential direction from the origin. The positions of the two accelerometers in the simulation are given in Table 2. The simulated signals that would be measured by the accelerometers attached in the axial and

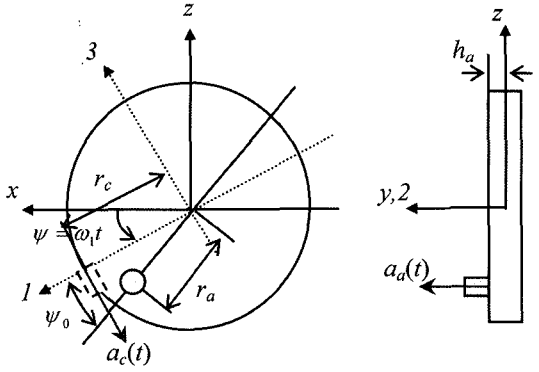

Figure 3. Positions of the accelerometers mounted in the circumferential and axial directions of a rotating disk.

Table 2. Position of the two accelerometers.

	accelerometer mounted in the axial direction	accelerometer mounted in the circumferential direction
r (mm)	r_a=18.8	r_c=23
y (mm)	h_a=10	0
offset angle ψ_o (°)	17	0

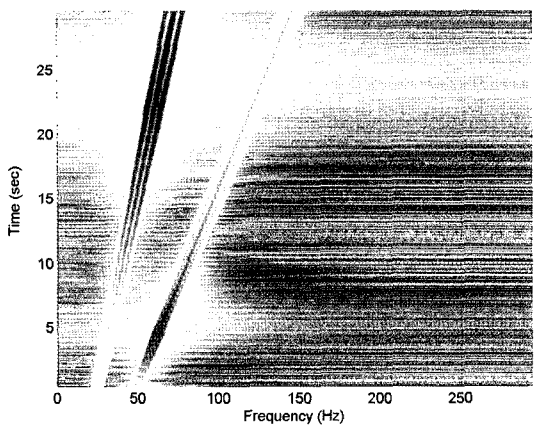

Figure 4. Spectrogram of the simulated acceleration signal for the accelerometer mounted in the axial direction.

circumferential directions can then be easily evaluated by substituting the synthesized vibration components calculated from Equation (23) into Equations (10) and (11), respectively.

The spectrograms of the simulated signal for the accelerometers attached in the axial and circumferential directions are shown in Figures 4 and 5, respectively. Since the amount of the Doppler shift in order is as small

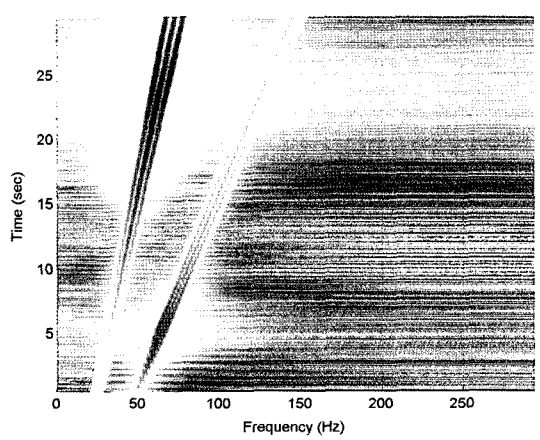

Figure 5. Spectrogram of the simulated acceleration signal for the accelerometer mounted in the circumferential direction.

as 0.1444, the Dopplerized order components, 1.8556 and 2.1444 orders, are shown to be closely placed to order 2, as is also the case for the Dopplerized orders of 4 (orders 3.8556 and 4.1444). To accurately retrieve the six components of vibration signals from the two accelerometer signals, it is therefore important to precisely decouple the close orders of interest.

3.2. Vold-Kalman Order Tracking Filter

The Vold-Kalman order tracking filter extracts phase-assigned orders or order waveforms as a function of time. It provides non-phase-biased orders by post-processing operations. Close orders can be extracted simultaneously while minimizing the coupling effects, which is one of the most important advantages over other methods for the present application. In the Vold-Kalman operations, three types of filter shapes are provided, which are 1-, 2-, and 3-pole filters. The higher the filter order, the better the filter selectivity is in the frequency domain. Two- or three-pole filters are usually preferred to avoid interference between orders. Readers who are not familiar with the Vold-Kalman filter are referred to a reference such as (Gade *et al.*, 1999).

For the operations, not only are the orders to be simultaneously extracted selected, but also the filter bandwidths for each order is specified. It is known that the wider in frequency the filter width, the shorter the filter response in the time domain, which thereby enables the filter to follow faster the change in the signal. The selection of bandwidth is thus a compromise between having a sufficiently narrow bandwidth to separate the close order components in the signal and having a bandwidth wide enough to follow the rapid change in the signal amplitude especially around a resonance peak. To ensure an error less than 0.5 dB of the peak amplitude at the resonance, the minimum filter bandwidth for the extraction of order k is known to be:

$$B_{3dB}=2/T_{3dB}, \tag{24}$$

where T_{3dB} is the time it takes for the order k to sweep through the 3-dB bandwidth of the peak, which can be represented as:

$$T_{3dB}=\Delta f_{3dB}/(k\times \mathrm{SR}_{\mathrm{RPM}}/60), \tag{25}$$

where Δf_{3dB} is the 3-dB bandwidth of a resonance peak, and can be calculated for a single degree-of-freedom vibration system as:

$$\Delta f_{3dB}=2\zeta f_n. \tag{26}$$

In the Vold-Kalman algorithm, either a constant filter bandwidth or a proportional filter bandwidth can be used. A proportional filter bandwidth is given as a percentage of the fundamental order (i.e., the engine speed), and is recommended for a higher-order analysis or an analysis

over a relatively wide rpm range. In the present work, proportional filter bandwidths are used. The minimum filter bandwidth for a non-Doppler shifted order, such as order 2, can be obtained straightforwardly by using Equations (24) to (26). For order 2, the minimum filter bandwidth that ensures an error less than 5 dB in the estimate of the peak resonance level is calculated to be 0.641 Hz. A bandwidth of 0.641 Hz for order 2 at the resonance frequency of 65 Hz corresponds to 1.97% bandwidth (i.e., 2×0.641/65).

Each of a pair of Doppler-shifted orders contains the other two vibration components of the three vibration components that one accelerometer can measure. For instance, the peak resonances of both the rotational vibration components about the x- and z-axes are observed in the order 1.8556 component of the signal measured by the accelerometer attached in the axial direction. The filter bandwidth should therefore be calculated based on the peak resonance that would result in a wider bandwidth. Since both the resonances have the same resonance frequencies and damping ratios in the present simulation, either resonance of the two vibration components can be taken. The time it takes for order 1.8556 to sweep through the resonance with the sweep ratio of 50 rpm/s can be calculated by substituting the Doppler-shifted resonance frequency (i.e., 60×1.8556/2) into Equation (26) and substituting the order 1.8556 into k in Equation (25). Note that substituting the non-Doppler-shifted order 2 into Equation (25) and the non-Doppler-shifted resonance frequency, 60 Hz, into Equation (26) would yield the same T_{3dB}, which is 2.88 sec. The minimum filter bandwidth at the resonance is then 0.6944 Hz, from Equation (24). A bandwidth of 0.6944 Hz for order 1.8556 at the Doppler-shifted resonance frequency (i.e., 60×1.8556/2 Hz) corresponds to 2.31% bandwidth (i.e., 1.8556×0.6944/60). This also corresponds to the bandwidth for the non-Doppler-shifted order number 2 at the non-Doppler-shifted resonance frequency, 60 Hz.

The rest of the minimum proportional filter bandwidths can be obtained similarly. Minimum bandwidths calculated for each order are given in Table 3. The magnitude of the phase-assigned orders extracted with a two-pole Vold-Kalman filter with bandwidths given in Table 3, and with bandwidths of double, triple, and quadruple of the bandwidths given in Table 3, are shown in Figure 6 for the input signal from the accelerometer attached in the axial direction, and in Figure 7 for the input signal from the accelerometer attached in the circumferential direction.

No observable interference between orders (which is usually observed where orders pass through resonances of other orders, especially when a low selectivity filter is used) is seen in both Figures 6 and 7. As the filter bandwidth increases, however, the estimated magnitude

Table 3. Values of the minimum proportional Vold-Kalman filter bandwidths obtained by Equation (24) for the simulation data.

order extracted	proportional bandwidth (%)	
	for signal shown in Figure 4	for signal shown in Figure 5
2	1.97	2.31
1.8556	2.31	1.97
2.1444	2.31	1.97
4	7.89	9.26
3.8556	9.26	7.89
4.1444	9.26	7.89

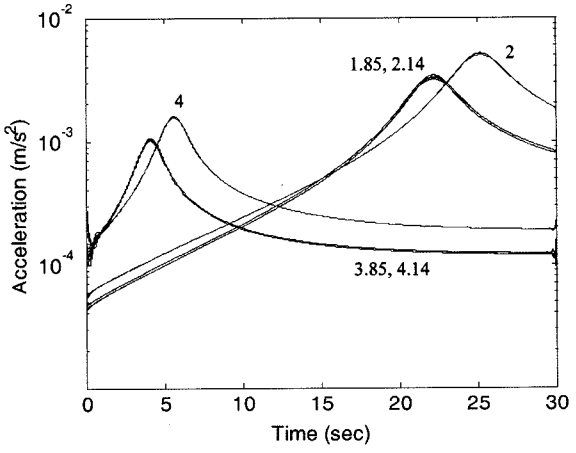

Figure 6. Magnitude of the phase-assigned orders extracted from the signal shown in Figure 4, with a two-pole Vold-Kalman filter with bandwidths in multiples (1, 2, 3, and 4) of those given in Table 3. Indicated numbers are the corresponding order numbers for each curve.

for higher orders begins to deviate from smooth curves either near the initial time (Figure 6) or near the end time (Figure 7), even though the general shapes of the magnitude of the extracted phase-assigned orders remains almost unchanged.

By using the procedure described in section 2.3, the six components of vibration signals were retrieved from the phase-assigned orders extracted with bandwidths of integer multiples up to ten of the minimum bandwidths given in Table 3. The estimation errors in the resonance levels are compared for: the sets of bandwidths, the translational acceleration in the y-direction, and the two rotational accelerations about the x- and z-axes (Figure 8); and the rotational acceleration about the y-axis, and the two translational accelerations in the x- and z-directions (Figure 9). It can be seen in Figures 8 and 9 that, with the minimum filter bandwidths given in Table 3

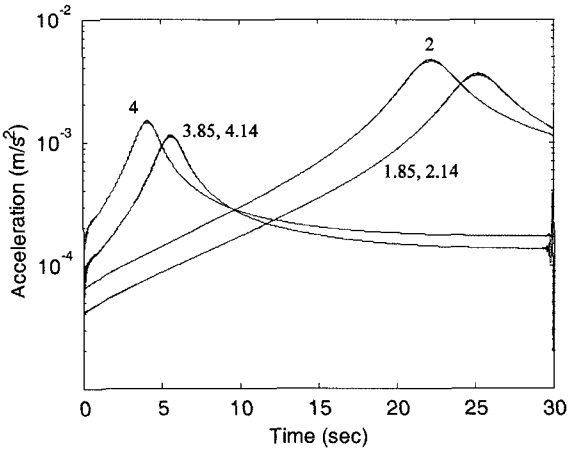

Figure 7. Magnitude of the phase-assigned orders extracted from the signal shown in Figure 5 with a two-pole Vold-Kalman filter with bandwidths in multiples (1, 2, 3, and 4) of those given in Table 3. Indicated numbers are the corresponding order numbers for each curve.

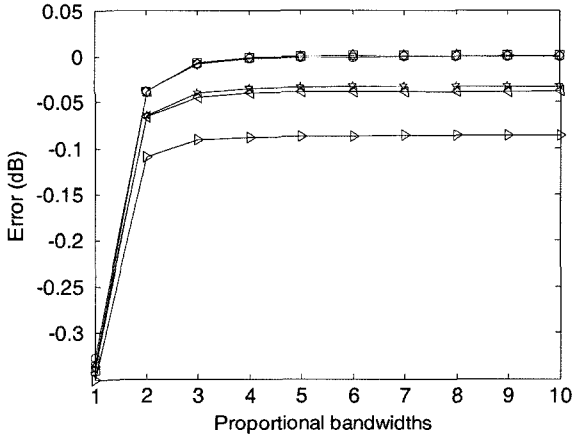

Figure 8. Errors in the vibration resonance level estimates (estimated resonance level minus true resonance level) as a function of the integer multiples of the filter bandwidths given by Table 3; second-order (circles) and fourth-order (right triangles) components of translational vibration in the y-direction; second-order (squares) and fourth-order (pentagrams) components of rotational vibration about the x-axis; and second-order (diamonds) and fourth-order (left triangles) components of rotational vibration about the z-axis.

the errors are already less than 0.35 dB. Furthermore, these errors decrease rapidly as the filter bandwidths increase and do not decrease much for bandwidths beyond four times those given in Table 3. In the present work, bandwidths of double the bandwidths given in Table 3 are chosen. The six components of vibration signals retrieved are shown in Figures 10 and 11 based on

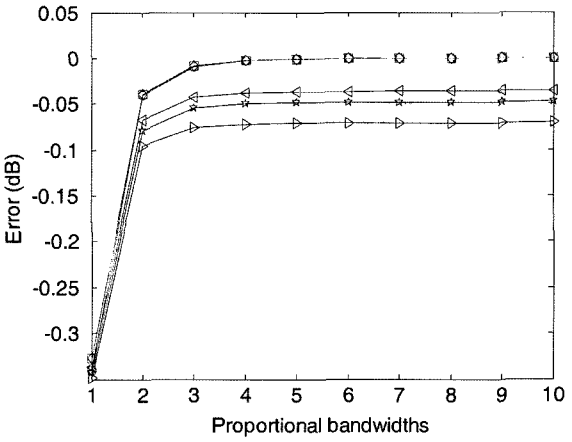

Figure 9. Errors in the vibration resonance level estimates (estimated resonance level minus true resonance level) as a function of the integer multiples of the filter bandwidths given by Table 3; second-order (circles) and fourth-order (right triangles) components of rotational vibration about the y-axis; second-order (squares) and fourth-order (pentagrams) components of translational vibration in the x-direction; and second-order (diamonds) and fourth-order (left triangles) components of translational vibration in the z-direction.

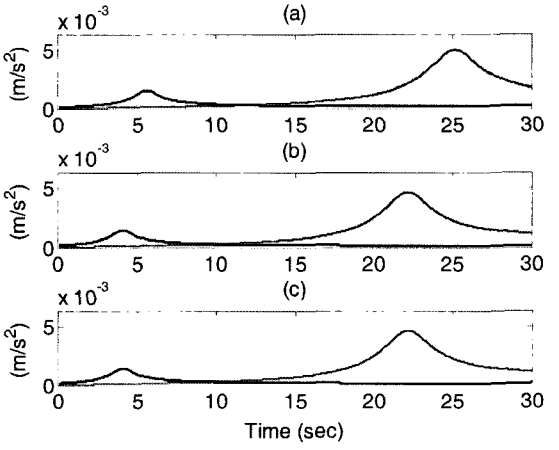

Figure 10. Comparison between the original signals created by a simulated run-up test and the retrieved envelopes of the vibration signals obtained by the procedure described in the present work: (a) for the translational acceleration in the y-direction; (b) for the rotational acceleration about the x-axis; (c) for the rotational acceleration about the z-axis. The envelopes for the second-order component are denoted by red lines, while those for the fourth-order component are denoted by black lines.

the selected bandwidths. The envelopes of the retrieved vibration signals correspond very accurately with the

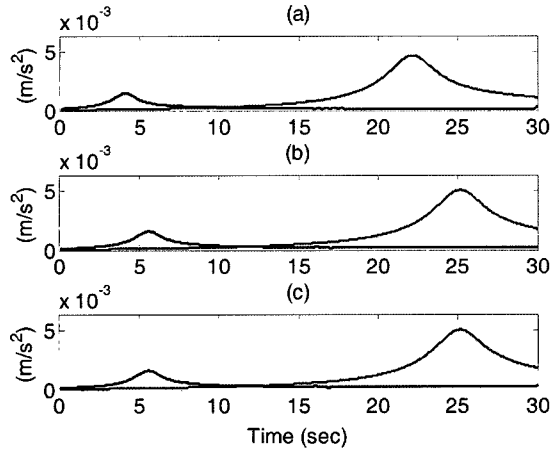

Figure 11. Comparison between the original signals created by a simulated run-up test and the retrieved envelopes of the vibration signals obtained by the procedure described in the present work: (a) for the rotational acceleration about the y-axis; (b) for the translational acceleration in the x-axis; (c) for the translational acceleration about the z-axis. The envelopes for the second-order component are denoted by red lines, while those for the fourth-order component are denoted by black lines.

original vibration signals.

4. APPLICATION TO A HALFSHAFT VIBRATION MEASUREMENT DATA

To obtain real vibration data from the halfshaft of a front-wheel drive, 4-cylinder, mid-size sedan, an aluminum ring adapter was made to attach accelerometers to the rotating halfshaft (Figure 12). The positions of the accelerometers in the simulated run-up test shown in Table 2 are in fact based on the design specifications of the aluminum ring adapter made in the present work. The aluminum ring adaptor assembly was attached in roughly the middle of the left halfshaft of the test vehicle (i.e., between the inboard joint and the outboard joint). Data acquisition from the rotating accelerometers was made possible by cabling through a slip ring. The vehicle run-up test was performed on a chassis dynamometer to simulate a plain road-load condition. The run-up test was performed with the 2nd gear, when the ratio of the rotating speed of the halfshaft to the engine speed was 0.1444:1. The engine speed was increased from approximately 2,500 rpm to 6,000 rpm at a nearly constant sweep ratio of approximately 313 rpm/s, and was measured by an engine tachometer as a function of time.

This vehicle run-up test is intended as a preliminary experiment to obtain real data to use in the de-Dopplerized vibration components retrieval procedure for demonstration purposes, while a detailed and full experimental study on the contribution of halfshaft vibration components to vehicle interior noise is left as future work. In the present work, the procedure for obtaining the corresponding three vibration components associated with the acceleration signal measured in the circumferential direction is demonstrated. The other set of three vibration components from the signal measured in the axial direction of the halfshaft can be in fact independently obtained using an identical procedure.

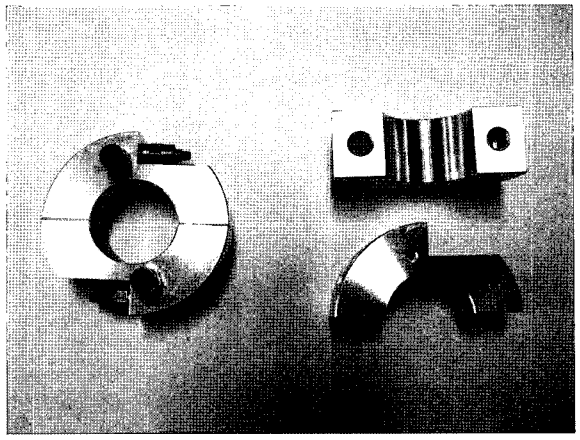

Figure 12. An aluminum ring adaptor used for measuring vibrations of a rotating shaft.

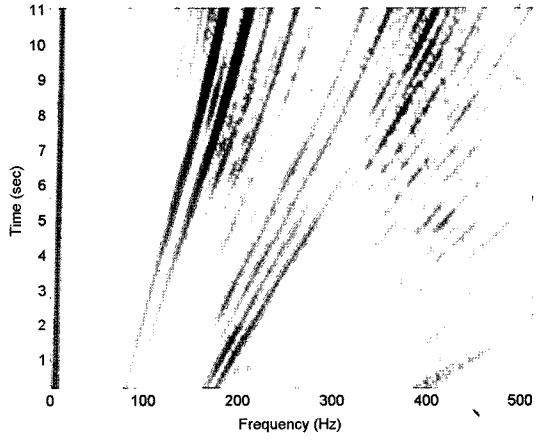

Figure 13. Spectrogram of the acceleration signal measured by the accelerometer attached in the circumferential direction of the aluminum ring adaptor.

A spectrogram of the acceleration signal obtained by the accelerometer attached in the circumferential direction of the aluminum ring adaptor during the run-up test is shown in Figure 13. For a 4-cylinder engine, the main firing orders are 2nd order and its inter multiples. By closely inspecting the spectrogram shown in Figure 13 and a spectrogram of the interior noise of the vehicle during the run-up test, orders 2, 3.5, and 4 are considered

Table 4. Values of the proportional bandwidths used in the Vold-Kalman operations for data obtained from experiment.

Order extracted	Proportional bandwidth (%)
2	3.2
1.8556	2.6
2.1444	2.6
3.5	9.85
3.3556	7.98
3.6444	7.98
4	12.86
3.8556	10.42
4.1444	10.42

to be main contributors to the interior noise. To calculate the bandwidths for the Vold-Kalman filter based on the procedure described in section 3.2, resonance frequencies of 200 Hz for the two translational vibration components and 180 Hz for the rotational vibration component were estimated based on the observation in Figure 13; a light damping ratio of 0.04 was assumed for all three vibration components. The three orders of interest and their Dopplerized pairs of orders, as well as the bandwidths used in the Vold-Kalman operations, are given in Table 4. The bandwidths specified in Table 4 are double the minimum bandwidths calculated by Equation (24).

The nine orders of interest were simultaneously extracted using the Vold-Kalman operations with a two-pole filter, and the magnitude of the extracted orders are shown in Figure 14. In Figure 15, the original signal and the sum of the extracted orders are compared. It can be

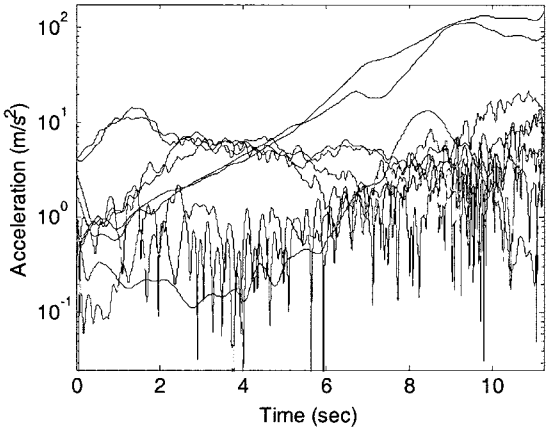

Figure 14. Magnitude of the phase-assigned orders extracted from the signal shown in Figure 13, with a two-pole Vold-Kalman filter with bandwidths given in Table 4. Indicated numbers are the corresponding order numbers for each curve.

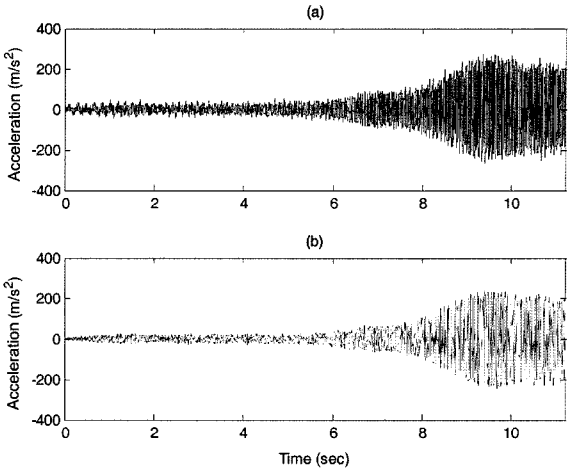

Figure 15. Comparison between (a) the signal shown in Figure 13 and (b) the sum of the order components extracted by Vold-Kalman operations.

seen that the sum of the major orders selected in the Vold-Kalman operations represents the characteristics of the original signal fairly well.

The rotational (or torsional, in this case) vibration components can be obtained directly from non-Dopplerized order components among the extracted orders (i.e., orders 2, 3.5 and 4). The magnitude of the phase-assigned orders for the rotational acceleration components are shown in Figure 16. The magnitude of the de-Dopplerized phase-assigned order for the two translational vibration components are shown in Figures 17 and 18. Interestingly, a beat phenomenon can be observed in the retrieved signal for the two translational vibrations. This beat occurs because the principal axis of the translational (or radial in this case) vibration rotates as a function of

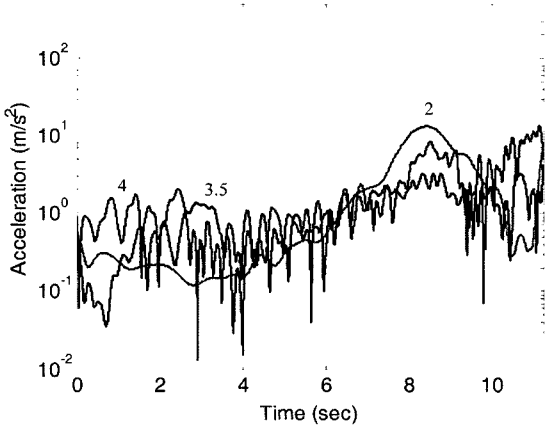

Figure 16. The envelopes obtained for the rotational acceleration about the y-axis. Indicated numbers are corresponding order numbers for each curve: order 2 (red line), order 3.5 (black line), and order 4 (blue line).

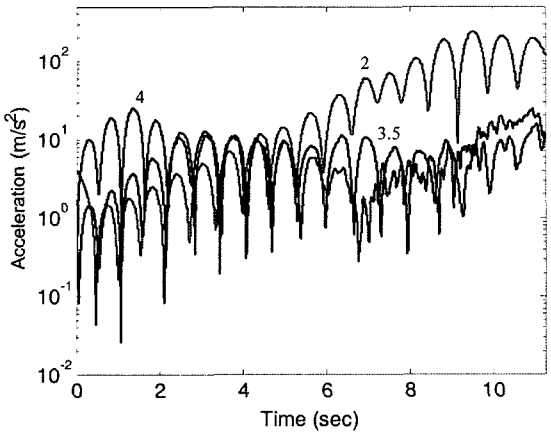

Figure 17. The envelopes of order components for the translational acceleration in the x-direction obtained by the procedure described in the present work. Indicated numbers are corresponding order numbers for each curve: order 2 (red line), order 3.5 (black line), and order 4 (blue line).

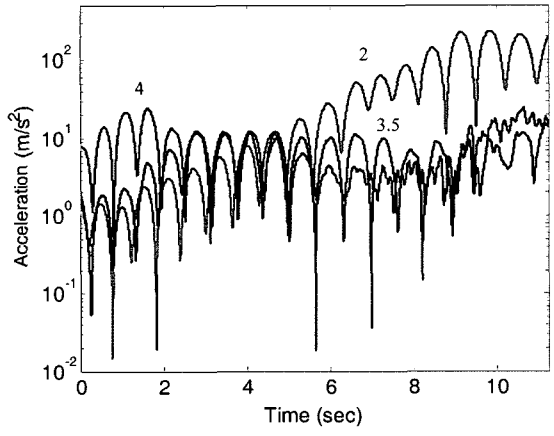

Figure 18. The envelopes of order components for the translational acceleration in the z-direction obtained by the procedure described in the present work. Indicated numbers are corresponding order numbers for each curve: order 2 (red line), order 3.5 (black line), and order 4 (blue line).

time. This can be verified by evaluating the magnitude of the total translational acceleration as a function of time as shown in Figure 19. Unlike the magnitude of each component of the translational acceleration, the total magnitude of the translational acceleration changes smoothly as a function of time. The mechanism that results in the slow rotation of the principal axis of the translational acceleration is unknown, but the period of the rotation is observed to be approximately 0.6 sec, and remained almost unchanged during the run-up test.

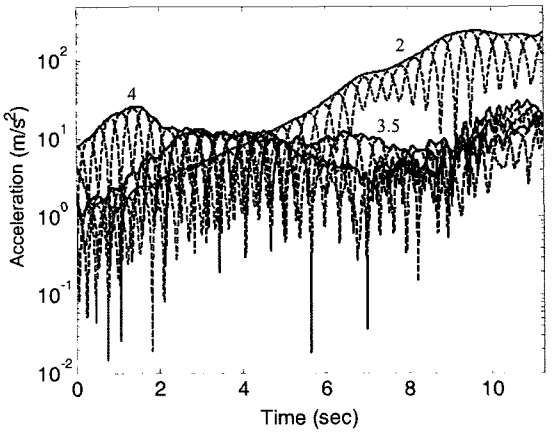

Figure 19. The envelopes of the total translational acceleration in a radial direction. Solid lines represent the total radial components, while dashed lines represent the radial components in the x- and z-directions shown in Figures 17 and 18, respectively. Indicated numbers are corresponding order numbers for each curve: order 2 (red line), order 3.5 (black line), and order 4 (blue line).

5. CONCLUSION

A new measurement method is proposed in the present work to enable order analysis of the six degree-of-freedom vibration components of a rotating shaft with only two accelerometers. This measurement method utilizes the spread of different vibration components in the spectrogram due to the Doppler effect. For a typical mid-size sedan operating in 2nd gear, the order shift of Dopplerized vibration components was approximately 0.1444. It was shown that these close orders can be resolved without much interference by using fine-order-resolution Vold-Kalman operations. The measurement method was applied to an order analysis of vibration components for a left halfshaft of a mid-size sedan. The preliminary results shows that the measurement and analysis method proposed in the present work can be a useful tool for order analysis of a rotating shaft.

ACKNOWLEDGEMENT–This work was supported by research program 2005 of Kookmin University in Korea.

REFERENCES

Gade, S., Herlufsen, H., Konstantin-Hansen, H. and Wismer, N. J. (1995). *Order Tracking Analysis.* Technical Review, **2**. B & K. Denmark.

Gade, S., Herlufsen, H., Konstantin-Hansen, H. and Vold, H. (1999). *Characteristics of the Vold-Kalman Order Tracking Filter.* Technical Review, **1**. B &K. Denmark.

Halliwell, N. A., Pickering, C. J. D. and Eastwood, P. G.

(1984). The laser torsional vibrometer: A new instrument. *J. Sound and Vibration* **93**, **4**, 588–592.

Halliwell, N. A., Hocknell, A. and Rothberg, S. J. (1997). On the measurement of angular vibration displacements: A laser tiltmeter. *J. Sound and Vibration* **208**, **3**, 497–500.

Miles, T. J., Lucas, M., Halliwell, N. A. and Rothberg, S. J. (1999). Torsional and bending vibration measurement on rotors using laser technology. *J. Sound and Vibration,* **226**, **3**, 441–467.

Rothberg, S. and Bell, J. (2004). On the application of laser vibrometry to translational and rotational vibration measurements on rotating shafts. *Measurement,* **35**, 201–210.

Suh, I.-S. and Orzechowski, J. (2003). Drivetrain torsional and bending vibration for a RWD vehicle interior noise development. *SAE Paper No.* 2003-01-1496.

Wang, P., Davies, P., Starkey, J. M. and Routson, R. L. (1992). A torsional vibration measurement system. *IEEE Trans. Instrumentation and Measurement* **41**, **6**, 803–807.

Williams, J. S. and Wilson, B. K. (1997). Measurement of the rotational vibrations of RWD output shafts and characterization of the resulting effect on passenger perceived noise. *SAE Paper No.* 972031, 1261–1268.